Magnetic Soft Continuum Robots With Braided Reinforcement

Peter Lloyd[1]*, Onaizah Onaizah[1], Giovanni Pittiglio[2],
Damith Katudampe Vithanage[1], James H. Chandler[1] and Pietro Valdastri[1]

***Abstract*— Flexible catheters are used in a wide variety of surgical interventions including neurological, pancreatic and cardiovascular. In many cases a lack of dexterity and miniaturization along with excessive stiffness results in large regions of the anatomy being deemed inaccessible. Soft continuum robots have the potential to mitigate these issues. Due to its enormous potential for miniaturization, magnetic actuation is of particular interest in this field. Currently, flexible magnetic catheters often rely on interactive forces to generate large deformations during navigation and for soft anatomical structures this could be considered potentially damaging. In this study we demonstrate the insertion of a high aspect ratio, 50 mm long by 2 mm diameter, soft magnetic catheter capable of navigating up to a 180° bend without the aid of forces of anatomical interaction. This magnetic catheter is reinforced with a lengthwise braided structure and its magnetization allows it to shape form along tortuous paths. We demonstrate our innovation in a planar silicone pancreas phantom. We also compare our approach with a mechanically equivalent tip driven magnetic catheter and with an identically magnetized, unreinforced catheter.**

I. Introduction

Soft continuum robots are an important avenue in overcoming the limitations of traditional steerable microcatheters for endoluminal interventions [1] [2]. Magnetically actuated continuum robots (MCRs) offer huge miniaturization potential and the prospect of safe navigation through small, sensitive and tortuous pathways [3] [4] [5]. Tip driven MCRs are established in the literature [6] [7] but are unable to actively shape form i.e. control their body shape independent of tip pose. This limitation is of particular concern when the navigation passes through unusually soft and sensitive tissue such as the pancreas [8] [9] or the brain [10] [11]. Shape forming capability could potentially avoid painful and/or damaging forces of anatomical interaction along the length of the MCR. Recently, MCRs which can shape form due to a variable magnetization profile along their length have been explored [12] [13] [14] [15], and our previous research demonstrated their efficacy for follow the leader navigations [16]. These MCRs have bespoke non-axial magnetization signatures which interact with applied magnetic fields to create torques and are thus capable of minimizing contact during forward motion [17]. This arrangement permits the use of far softer materials as reduced interaction allows for lower insertion forces - the stiffness of a traditional catheter is driven by the requirement to resist buckling under these insertion forces.

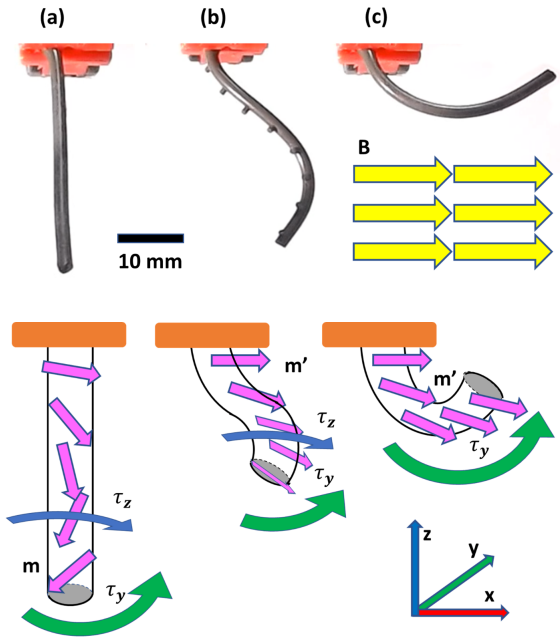

Fig. 1: (a) The referential (undeformed) MCR showing resultant torques about the Y axis (green) and the Z axis (blue) as a consequence of the interaction between applied field (B, yellow arrows) and magnetization profile (m, purple arrows) (b) Compound bending and twisting of an unreinforced CR. The welts placed along the back of the MCR clearly illustrate the twisting in the experimental domain. (c) Pure bending of a braid reinforced (torsionally constrained) MCR under identical magnetization profiles and applied actuating field (B_x = 20 mT).

However, a fundamental limitation of this non-axial magnetization design arises when a shape-forming MCR attempts to navigate a path featuring large (90° degrees or more) deformation. As described in detail in [18], in order to generate large deformations, the applied magnetic field must oppose the MCR's magnetization generating an inverted pendulum instability. If unconstrained, in accordance with Timoshenko beam theory, the much lower energy pose available via twisting around the catheter's long 'easy' axis will result

Manuscript received: April, 8, 2022; Revised June, 17, 2022; Accepted July, 1, 2022.

This paper was recommended for publication by Editor Yong-Lae Park upon evaluation of the Associate Editor and Reviewers' comments. Research reported in this article was supported by the Engineering and Physical Sciences Research Council (EPSRC) under grants number EP/R045291/1 and EP/V009818/1, and by the European Research Council (ERC) under the European Union's Horizon 2020 research and innovation program (grant agreement No. 818045). Any opinions, findings and conclusions, or recommendations expressed in this article are those of the authors and do not necessarily reflect the views of the EPSRC or the ERC.

(1) Storm Lab, School of Electronic and Electrical Engineering, University of Leeds, UK, {* men9prl}@leeds.ac.uk (2) The Department of Cardiovascular Surgery, Boston Children's Hospital, Harvard Medical School, Boston, MA 02115, USA

Digital Object Identifier (DOI): see top of this page.

(Figure 1b and supporting video). This unstable phenomenon is increasingly problematic as the aspect ratio of length to diameter increases.

Closed loop control such as [19] could theoretically counteract this instability however this would require accurate, high frequency feedback from inside the body of both bending and twisting deformations, which currently represents a major challenge. Mechanical reinforcement is an alternative and more practical approach and was introduced to a large diameter (6 mm) MCR design in the form of double helix fibers [18]. This approach demonstrated significant improvement but proved difficult to miniaturize due to its complex fabrication process.

In this paper, we demonstrate the successful harnessing of magnetic instability into large deformation shape forming by reinforcing a high aspect ratio, 50 mm long x 2 mm diameter catheter using a braided structure along its length. The braid we employ is a commercially available, 1 mm external diameter nylon cord. In Section II-C, we use it to experimentally demonstrate an increase in twisting stiffness that is 20 times the increase in bending stiffness. We demonstrate the practical advantage of this approach through autonomous follow-the-leader navigation into the pancreatic and bile ducts of a planar soft gelatinous phantom. This represents a continuation of our earlier work ([18]), but the proposed MCR design is 3 times smaller and exhibits a far higher ratio of twisting to bending stiffness. These improvements result in the first demonstration of such large deformations being generated during the insertion process without the requirement of forces of anatomical interaction. In particular, this absence of these forces represents a significant step forward in the development of atraumatic follow-the-leader MCRs. Furthermore, we demonstrate the inability of either a tip driven MCR or a similarly lengthwise magnetized but unreinforced MCR to achieve similar navigations when interactive forces are not available.

II. The Braided Catheter

In this section, we detail the model, fabrication method and characterization of our prototype braided MCR, actuated in a 1-D homogeneous field. The design principle is to utilize the anisotropic material response of an embedded braid to reduce instability under opposing field-magnetization conditions. Using the braid as a mechanical constraint, axial stiffness is increased relative to bending stiffness. As such we develop a rigid-link model to consider these independent stiffness parameters as a function of the catheter's length. Through characterization of fabricated samples in a 1-D field, we determine these relative stiffness parameters to allow for optimization of mechanically reinforced designs in more realistic scenarios.

A. Rigid Link Robot Model

In order to capture anisotropic behavior, we represent our MCR as a serial chain of five rigid links each 10 mm long and connected by a three Degree-of-Freedom (DoF) sprung rotational joint. The three DoFs in each homogeneous

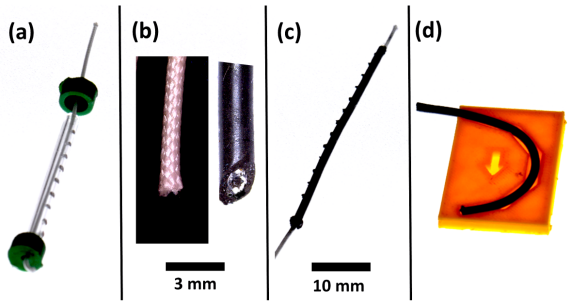

Fig. 2: (a) The 1 mm diameter nylon braid is secured in a 2 mm internal diameter perspex tube. This is injected with NdFeB doped Ecoflex-0030 and time cured. (b) Magnified images of the 1 mm diameter braid (white on a black background) and a diagonal cut of the 2 mm diameter MCR after casting (black on a white background with the embedded braid seen as a white circle). (c) The reinforced MCR is delaminated and trimmed to size. (c) This can then be magnetized in any direction desired. In the example shown it is being prepared for the demonstration in Section II-D.

rotational joint represent bending about the local X axis, bending about the local Y axis and twisting about the local Z axis, respectively. This characterization is repeated identically for each of the five rigid links such that any desired 50 mm path can be kinematically represented as a 5 x 3 array of joint angles Q. This allows the design to consider quasi-static insertion over discrete time steps.

A magnetic dipole with moment $\mathbf{m}$ in a homogeneous field $\mathbf{B}$ will experience a resultant magnetic torque linearly proportional to applied field strength

$$\boldsymbol{\tau} = \mathbf{m} \times \mathbf{B} \tag{1}$$

where $\mathbf{B}$, $\mathbf{m}$, $\boldsymbol{\tau} \in \mathbb{R}^3$.

The body torque acting on any given finite volume of the MCR as a consequence of the interaction of the actuating magnetic field and the magnetization of that region of doped elastomer will produce deformation and therefore be counteracted by the elastic properties of the material. The deformation resulting from balancing magnetic and elastic torques is represented as the joint angle array (Q) which explicitly defines both the tip pose and the body shape of the MCR.

Under a three dimensional rigid link assumption, as detailed in [17] and according to [20] [21], we balance the magnetic and mechanical torques across all 15 joints in the MCR at any given time step

$$J^T \boldsymbol{\tau} - KQ = \lambda \tag{2}$$

with J^T the Jacobian transpose of the MCR, $\boldsymbol{\tau}$ the magnetic torque from Equation 1 (both calculated at the desired joint angles, Q), K the stiffness matrix and λ the residual error in the torque balance: zero for a stable arrangement.

For the sake of simplicity, and due to the principle demonstration being performed in a low friction horizontal plane, gravity has been set to zero in this calculation. Gravity was incorporated in the corresponding theoretical framework in [17] and was found to impart less than 20% of the

magnitude of the magnetic torque (in a vertically aligned demonstration).

To construct the stiffness matrix for each identical 3 DoF joint, we assume linear elasticity such that

$$K = \text{diag}(E_x I_x \; E_y I_y \; E_z I_z) \tag{3}$$

where E_x, E_y and E_z are the Young modulus in the three directions (equal to E for an isotropic continuous medium, Section II-C gives details on anisotropic characterization), I_x and I_y second moment of area for bending and I_z second moment of area for twisting [20].

By summing the errors (λ) across all rigid links and all insertion time steps, a single function to be minimized is defined with the 5 x 3 arrays **m** and **B** as objective variables. This was solved as in [17] using the Genetic Algorithm (GA, Global Optimization Toolbox, Matlab version R2021b, the MathWorks, Natick, MA, USA) to generate suites of magnetizations and actuating fields specifically for each set of joint angles and stiffness matrices.

B. Fabrication

In order to test our MCRs, we developed a fabrication process as outlined in Figure 2. A nylon braid of external diameter 1 mm (Everlasto - James Lever 1856 Ltd, Manchester, UK) was held in axial alignment within a 2 mm internal diameter perspex tube using 3D printed end-caps ((RS-F2-GPGR-04, Formlabs, USA). The tube was pre-drilled with 0.5 mm diameter holes at 5 mm center spacings to give a clear indication of which side is the 'front' of each catheter - this welted effect can be clearly seen in Figure 1b. The elastomer (Ecoflex-0030, Smooth-On Inc, USA) was mixed with neodymium-iron-boron (NdFeB) microparticles with an average diameter of 5 μm (MQFP-B+, Magnequench GmbH, Germany) in a 1:1 mass ratio. This composite was mixed and degassed in a high vacuum mixer (ARV-310, THINKYMIXER, Japan) at 1400 rpm, 20.0 kPa for 90 seconds. The mixture was injected into the tubing and cured at room temperature for four hours before removal giving specimens as shown in Figure 2d.

Upon removal from the mold, the specimens were secured into a bespoke 3D printed magnetizing tray (Figure 2d) before being subjected to a saturating uniform field of 4.644 T (ASC IM-10-30, ASC Scientific, USA). The specific geometry of the magnetizing tray is determined according to the algorithm described in Section II-A and in [17].

C. Elastomeric Characterization

In order to optimize the rigid link model and determine the required magnetizations and actuating fields we must populate the stiffness matrix, K (Equation 3). As stated in Section II-A, in the case of the unreinforced MCR, this material response is exclusively generated by the isotropic bulk elasticity of the doped silicone. However, for a braid-reinforced MCR we must allow for deliberately inbuilt anisotropy in the response to actuation. The braid is constructed of multiple interwoven helical threads, which interact to constrain shear deformations at the local level whilst permitting normal deformations. Being positioned at (or near) the radial extremities of the MCR, these local constraints translate into globally constrained twisting whilst globally permitting bending [18] [22]. Pure bending and pure twisting characterization experiments were therefore performed, as illustrated in Figure 3.

TABLE I: Linearized pseudo elastic moduli for unreinforced and reinforced specimens of doped Ecoflex-0030. Note the torsionally constraining effect of the braid (20:1, twisting:bending stiffness) and the five-fold increase in MCR bending stiffness due to addition of the braid.

	E_x	E_y	E_z	E_z/E_x
Unreinforced Sample (kPa)	100	100	100	1
Reinforced Sample (kPa)	500	500	10,000	20

Samples were prepared in accordance with the method introduced in Section II-B with radial magnetization for the twisting samples and axial magnetization for the bending samples [18]. Three identical versions of each sample were hung vertically and exposed to an orthogonal 1-D field ramped from -25 mT to 25 mT for three repetitions each. Primitive deformations were analyzed using the MATLAB imtool functionality giving the graph shown in Figure 3 relating applied field (**B**) to tip deformation angle (q) for a 20 mm specimen length (L). From the relationship

$$K\frac{q}{L} = |\mathbf{m} \times \mathbf{B}| \tag{4}$$

we established the stiffness parameters in Table I. Despite the obvious increase in bending stiffness our MCR is still flexible compared with other soft magnetic catheters in the literature, for example, the PDMS (Polydimethylsiloxane) + NdFeB (20 % volume fraction) as prepared and employed in [7] has an effective elastic modulus of E = 1,400 kPa.

D. Shape Forming in Free Space

To illustrate the impact of the inclusion of the braid on torsional stability and resulting deformation angle, two otherwise identical 40 mm samples (unreinforced and braid-reinforced) were fabricated and magnetized with the planar sinusoidal magnetization shown in Figure 1 (purple arrows). This magnetization was derived using the optimization algorithm described in Section II-A, but constrained to only the final time-step of insertion and a 1-D field B_x = +20 mT. The joint angle array was simply specified as the largest possible angle of bending about the Y axis, zero about the X and Z axes. The sinusoidal magnetization which emerged from this process reconciles with intuition.

When exposed to a 1-D field B_x = +20 mT (yellow arrows) both prototypes *should* produce large in plane deformation. Figure 4 shows the expanded time stepping view of the result shown in Figure 1 and in the supporting video. The braid is clearly needed in order to stabilize the actuation and effectively convert this magnetic torque into large (greater than $100°$) elastic deformation. As can be clearly seen the impact of anisotropic reinforcement is so profound as to be difficult to quantify - a maximal difference in tip orientation of $\approx 150°$.

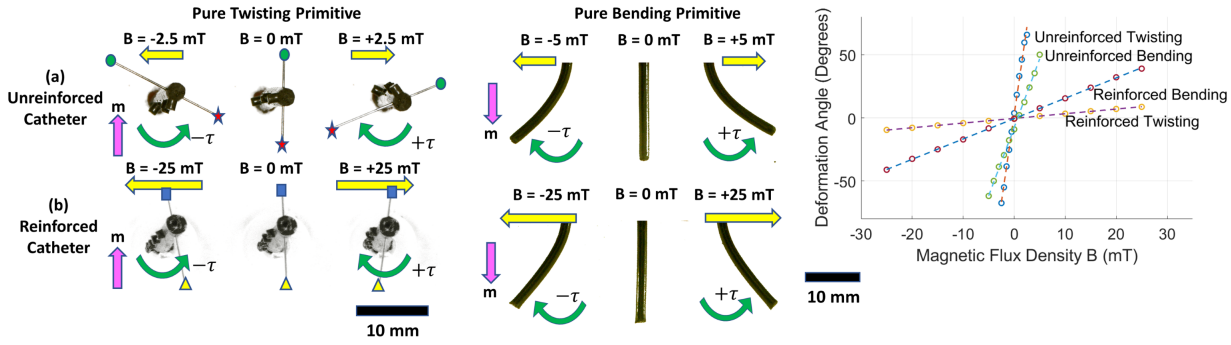

Fig. 3: Testing of primitive deformations for elastomeric characterization. Under pure twisting (left), radially magnetized 20 mm specimens are hung vertically and exposed to an orthogonal homogeneous field. The view shown is from below of (a) unreinforced catheter and (b) reinforced catheter (the tip has been pierced with a 0.25 mm diameter nitinol wire to aid visualisation and postprocessing). Under pure bending (centre), similar but axially magnetized specimens are hung vertically and the view shown is from the side. The graph (right) shows the curves of actuating field against angle of deformation. The reinforcing increases bending stiffness by around 5 times and twisting stiffness by around 100 times. The difference in curve gradient between twisting and bending for the isotropic, unreinforced specimen is due to the difference in second moment of area for the two deformations.

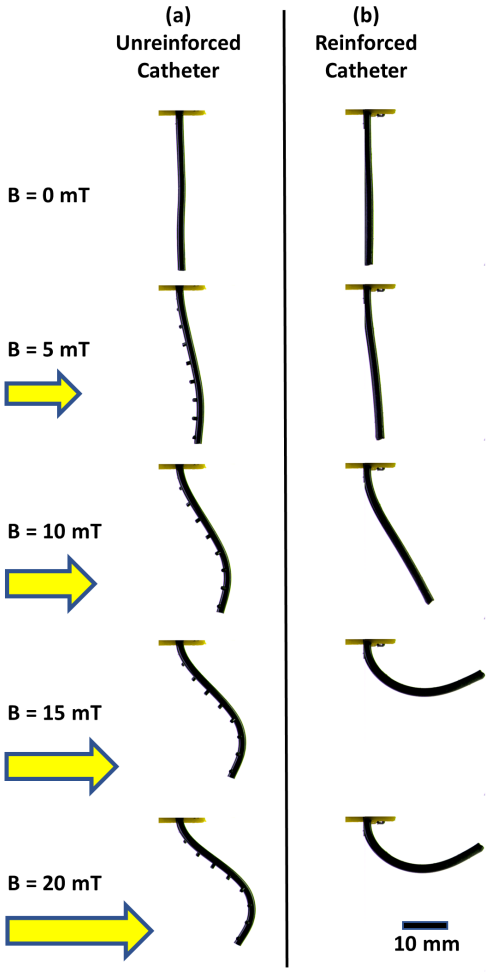

Fig. 4: Elastomeric deformation under 1-D homogeneous actuation. Magnetization is as depicted in Figure 1 (purple arrows) and Actuating Field B_x (yellow arrows) is ramped from 0 to 20 mT. (a) The twisted response of the unreinforced MCR. (b) The stable, constrained, and large deformation response of the braided MCR. These results are further demonstrated in the supporting video

This result allows the incorporation of previously unstable opposing field-magnetization combinations within the optimization solution. This in turn permits the possibility of higher bending angles and therefore successful low contact navigation through more tortuous pathways than previously possible.

III. Demonstration of Clinical Application

The ability to achieve large deformation shape forming may be useful in a large variety of clinical applications. One such application is catheterization of the notoriously soft and delicate pancreas [23]. To illustrate the potential for clinical relevance of our innovation, we performed navigations into the bile and pancreatic ducts of a planar, ultrasoft pancreas phantom. We compare these navigations with mechanically similar attempts using a tip driven MCR and an unreinforced length-wise magnetized MCR.

Current surgical catheters for pancreatic intervention have a minimum elastic modulus in the region of 2 GPa [24] in order to transfer longitudinal driving forces around the necessary internal corners at an appropriate scale and without buckling. This is 500,000 times stiffer than pancreatic tissue [9] and more than 4000 times stiffer than the catheter we have developed.

A. Path Planning

Utilizing anatomical data from the turbosquid dataset (www.turbosquid.com) (Figure 5a) we extracted center lines of the pancreatic and bile ducts (Figure 5b) using 3DSlicer (www.slicer.org). These center lines give desired pathways from a start point in the duodenum to a location 50 mm distal in either duct. These point cloud trajectories can be characterized as 5 x 3 arrays of joint angles (Q) in accordance with the rigid link assumptions described in Section II-A. The redundancy in the mapping between trajectory and joint angles arising due to the lack of orientation about the local Z axis in the trajectory data is managed by minimizing deformed strain energy. This calculation is a function of the stiffness matrix (Equation 3) and, due to the deliberately isotropic design (Section II-C), results in near zero twist.

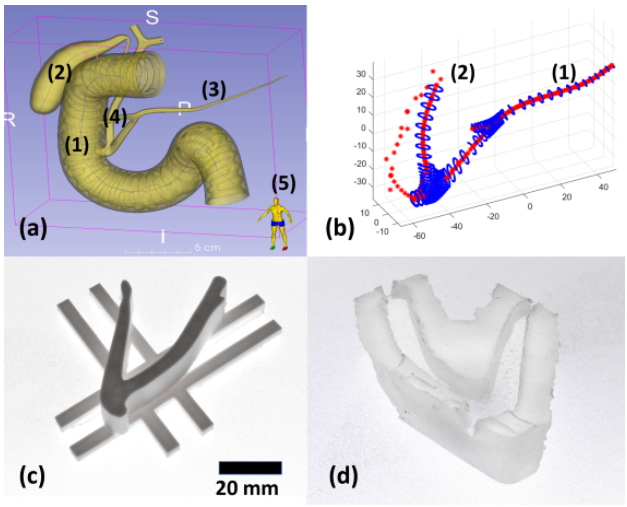

Fig. 5: (a) The initial 3-D geometry of (1) duodenum, (2) gall bladder, (3) pancreatic and (4) bile ducts. The character at (5) shows the relative orientation of this anatomy. (b) The point-cloud (blue) of the area of interest: (1) pancreatic and (2) bile ducts. Center lines for path planning are shown in red. (c) The 3-D printed PLA imprint prior to casting - this is shown upside down for the sake of visibility. (d) The 5 kPa soft silicone phantom running from the major papilla into the ducts.

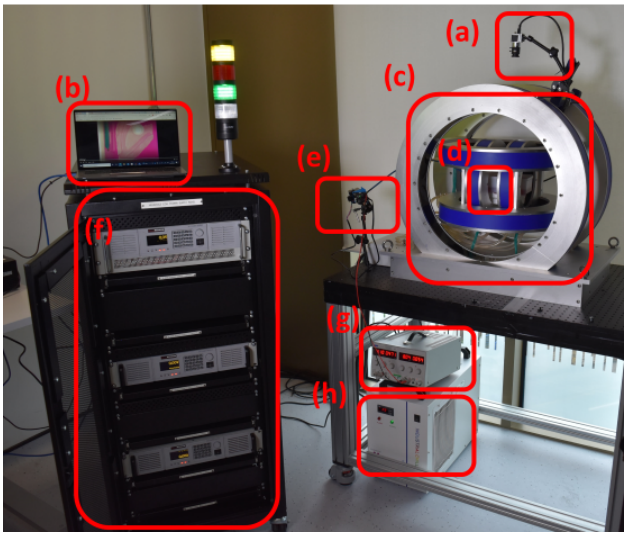

Fig. 6: The 3D Helmholtz coil based actuation platform as described in Section III-C. (a) Basler camera, (b) cpu (c) 3D Helmholtz coil, (d) 3D work space - site of experimental arrangement, (e) stepper motor, (f) 3 power supplies for Helmholtz coils, (g) power supply for stepper motor, (h) coolant tank for Helmholtz coils.

Consequently, a unique, minimum strain energy joint angle array can be used to supply the optimization described in Section II-A. During navigation these links were sequentially inserted over five discrete time steps under the quasi-static assumption.

B. Soft Phantom

The soft phantom used for demonstration of our method utilizes anatomical data from the aforementioned turbosquid dataset. This provides accurate external geometry of the bile duct, pancreatic duct and common duct. The internal geometry of the duct network (Figure 5b) was scaled according to [25] which gives a bile duct maximal internal diameter of 7 mm. This scaling compensates for any inaccuracies in wall thicknesses of the original imaging. Furthermore, we have included a major papilla at the outlet of the drainage duct with a minimum diameter of 2.6 mm [26]. These combined dimensions were projected onto a sketch plane, extruded 20 mm, 3D printed (RS-F2-GPGR-04, Formlabs, USA) (Figure 5c) and then open-cast in silicone: 2 parts SoftGel A-341C to 3 parts DC200 silicone oil (50 cst) (www.dow.com/en-us) for 4 hours in accordance with [27] (Figure 5d). This gives an approximate linearized elastic modulus of E $\approx$ 5 kPa for strains of less than 10% which reconciles with the E $\approx$ 3 kPa for healthy pancreatic tissue given in [9]. During navigation the channel was lubricated with dyed water to reduce friction and aid visualization. We consider this approach an effective demonstrative environment and the open channel approach also allows for maximum visibility.

C. Actuation

A 3-D Helmholtz coil (3DXHC12.5-300, Dexing Magnet Tech. Co., Ltd, Xiamen, China) was used with a 60 mm cubed homogeneous workspace which can generate 3 linearly independent uniform magnetic fields up to 30 mT (Figure 6). These electromagnetic coils are connected to three independent power supplies (DXKDP, Dexing Magnet Tech. Co., Ltd, Xiamen, China) for each of the spatial axes. Power supplies connect to a PC from an RS232 serial communication port allowing control via MATLAB serial commands. A code is thus implemented to autonomously operate power supply output generating the desired 3D homogeneous magnetic fields.

The insertion motor consists of a Nema 17 stepper motor (Micromech, UK), a 3D printer extrusion head minus the nozzle and is controlled using a UStepper S (http://ustepper.com) stepper motor driver. This drives a 1.75 mm diameter PLA filament through a 2.5 mm internal diameter bowden cable sleeve to the insertion origin (as in Figure 7). The proximal end of the MCR is attached to the distal end of the filament using 2.5 mm diameter thermal shrink fitting sleeve. The stepper driver receives directional commands via a fourth serial port again operated from the same MATLAB code. Step count is proportional to the advance length of the inserter which was reconciled offline. Therefore, by controlling the step count and operating frequency, the inserter can extend and retract the MCR autonomously with known length and speed. In this case the inserter was programmed to extend the MCR with 1 mm increments synchronized to changes in actuating magnetic field. The entire system is capable of operating at a frequency of 2 Hz meaning a 50 mm navigation takes 25 seconds.

Experiments in the 3D coil were recorded using a top-view Basler Ace camera (acA2040-120uc Basler AG, Ahrensburg, Germany) with a Basler C23-3518-5M-P f35mm lens. Images and videos in the 1D trial were recorded similarly using a side-view camera.

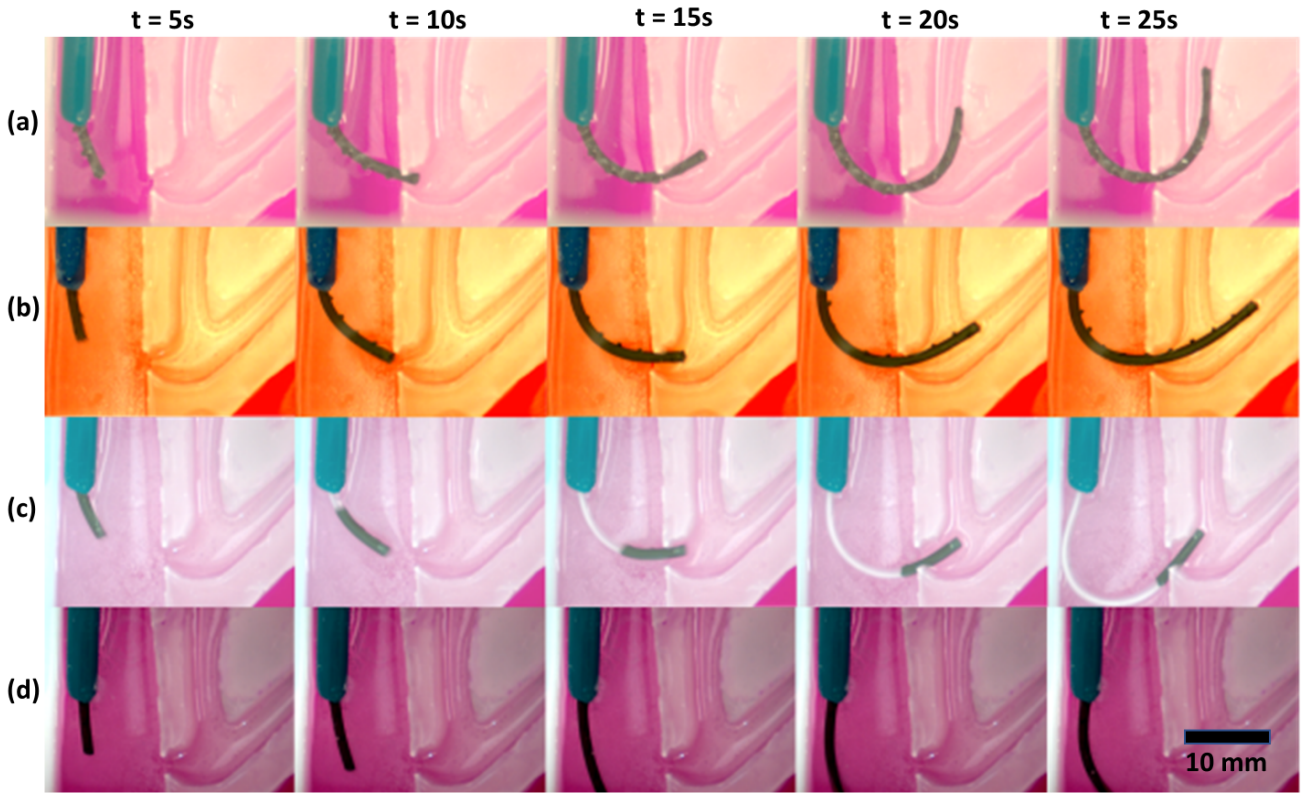

Fig. 7: Navigation into the bile and pancreatic ducts - stills taken from the supporting video. Magnetizations and actuating fields are shown in the supporting video. (a) An optimized, reinforced MCR navigating into the bile duct. (b) An independently magnetized, reinforced MCR navigating into the pancreatic duct. (c) A tip driven MCR attempting to navigate into the pancreatic duct (d) An optimized, unreinforced MCR attempting to navigate into the pancreatic duct.

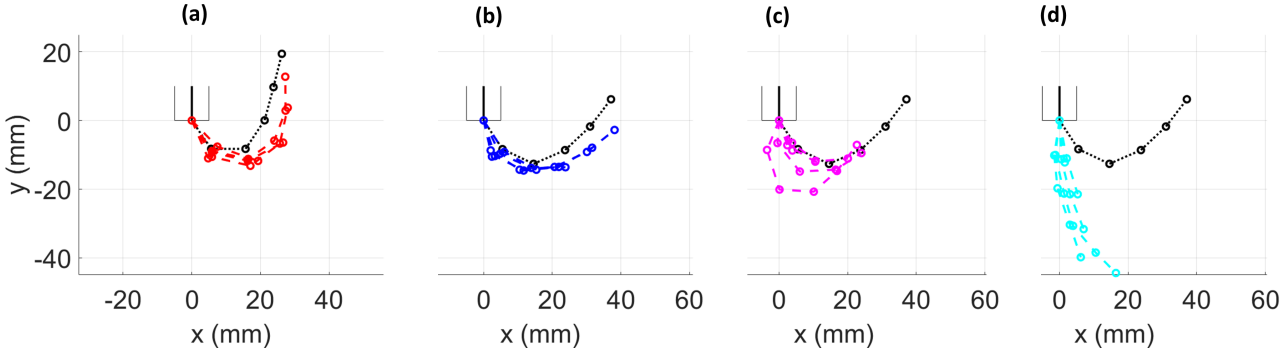

Fig. 8: Desired path (black hatchings) against experimental data for (a) optimized navigation into the bile duct (red hatchings), (b) optimized navigation into the pancreatic duct (blue hatchings), (c) tip driven navigation into the bile duct (purple hatchings), (d) optimized but *unreinforced* navigation into the bile duct (turquoise hatchings). Position after each of five time increments for one experimental repetition are shown. Mean absolute spatial error calculated across all time steps and across all three experimental repetitions are (a) 4.7 mm, (b) 4.2 mm, (c) 9.1 mm and (d) 21.3 mm.

IV. Results

Figure 7 shows the five time steps of insertion into the pancreatic and bile ducts. These are all also shown in the supporting video. Figure 7a shows an optimized, reinforced MCR navigating 50 mm into the pancreatic duct. Figure 7b shows an independently optimized and therefore differently magnetized, reinforced MCR navigating 50 mm into the bile duct. Figure 7c shows a mechanically equivalent tip driven MCR attempting to navigate into the pancreatic duct. Actuating fields for this navigation were derived in exactly the manner described in Section II-A but with magnetization constrained to the tip driven arrangement. Figure 7d shows an unreinforced MCR, independently optimized to account for variation in material properties, attempting to navigate into the pancreatic duct. All insertions ran at 2 mm/s which represents an operating frequency of 2 Hz. All experiments were repeated three times under identical conditions.

Figure 8 shows the graphical representation of the same results. Desired path (black hatchings) against experimental data for Figure 8a optimized navigation into the bile duct (red hatchings), Figure 8b optimized navigation into the pancreatic duct (blue hatchings), Figure 8c tip driven navigation

into the bile duct (purple hatchings), Figure 8d optimized but *unreinforced* navigation into the bile duct (turquoise hatchings). Mean absolute spatial error calculated across all time steps and across all three experimental repetitions are (a) 4.7 mm, (b) 4.2 mm, (c) 9.1 mm and (d) 21.3 mm.

V. Discussions and Future Work

For any scenario where the anatomy through which we are attempting to navigate is narrow and significantly softer than the catheter, and where deformation angles of greater than 90° are required, conventional mechanical and tip driven systems will be either ineffective or traumatic (or both). Here we show that a 2 mm diameter, length-wise optimally magnetized MCR, with braided reinforcement, can reach otherwise inaccessible locations.

There is still spatial error in the two successful navigations which can be attributed to the imprecise positioning of the origin of the MCR - the insertion point. This error affects the joint angle array and thus the required actuating fields. In order to minimize this error we intend to incorporate a shape based closed loop control algorithm in our future work which can recalculate required joint angles based on strain sensor feedback such as Fiber Bragg gratings.

We are aware that the NdFeB used in our demonstration is potentially cytotoxic. This is a problem which can be readily solved by coating the magnetic continuum robot with biocompatible materials such as silica, parylene [28] or hydrogel [7] and has been widely demonstrated in the literature.

The manner of failure of the tip driven MCR is interesting. By pushing from the base of a manipulator, forward motion in the opposite direction can only *ever* be achieved if (1) interactive forces are present and (2) the manipulator is sufficiently rigid to transmit these forces to the tip. In our demonstration, the ultrasoft phantom will not permit interactive forces of any significance, as pancreatic or brain tissue would not, and the MCR is too soft to transfer them even if it would.

The unreinforced MCR is also unsuccessful in its navigation. Whilst it is imperceptible to the naked eye (due to the speed at which this failure occurs), this is entirely attributable to the twist detailed in Section II-D, in Figure 1 and in the supporting video. Mechanically unconstrained torque about the long Z axis induced by the unstable combination of magnetic fields causes the MCR to twist. This near 180° rotation of the plane of magnetization changes the profile of cross products and therefore magnetic body torques along the MCR. Deformation is thus reduced but also, the equilibrium calculations detailed in Section II-A are undermined. This results in a loss of correspondence, for the desired joint angles, in the elastic-magnetic torque balance of the MCR. The failures of both the tip driven and the unreinforced MCRs corroborate our claim that a torsionally reinforced catheter enables otherwise impossible shape-controlled, magnetic navigations.

The authors assumed, due to the successful implementation of the quasi-static assumption under insertion, that at a sufficiently low frequency, the operational code could simply be run backwards to give contact free *retraction*. As can be observed in the supporting video, for the larger deformation bile duct navigation, this is not true and significant phantom deformation occurs. The quasi-static assumption does not consider any driving force at the base of the MCR (as this would generate time dependency) which, for the retraction phase is clearly (and unexpectedly) critical. To address this interesting research question we believe the answer is to implement 'gradient pulling' - tangential pulling forces associated with magnetic field gradients.

We also anticipate developing a fabrication technique to produce narrower and more malleable braids to reduce bending stiffness E_x, E_y. Incorporated into this is the desire to better understand the theoretical role of the braid and its design parameters: material, helix angle, number and thickness of threads. We currently have a nylon braid wound at an angle of 35° from the longitudinal axis, but an unknown number and thickness of threads. Optimization of these parameters was explored in our earlier work on helical fiber support [18], but here we have utilized a commercial braid. As previously noted, this option offers a significant advantage in terms of miniaturization and reliability of fabrication but also exhibits major drawbacks in terms of control over these braid design parameters. By developing our own sub-millimetre scale braid fabrication we can optimize design parameters to further improve performance towards our target clinical application.

Finally, we also want to extend our demonstration into three dimensions to enable navigation through more convoluted routes such as those in the neurovascular network and deeper into the pancreas.

We have demonstrated a successful constraining of the twisting instability of MCRs under certain necessary configurations of magnetization and applied field. This has allowed us to achieve magnetically actuated, follow-the-leader navigation into an ultrasoft pancreatic phantom. This combination of large deformation and minimal reactive force has not previously been shown. With this contribution we have taken a significant step towards fulfilling the potential of shape forming MCRs for navigation through sensitive and convoluted anatomies in a safe, stable and repeatable manner.

Acknowledgement

The authors wish to thank Samwise Wilson and Vittorio Francescon for their technical assistance in developing the experimental arrangements used in this work.

References

[1] J. Burgner-Kahrs, D. C. Rucker, and H. Choset, "Continuum robots for medical applications: A survey," *IEEE Transactions on Robotics*, vol. 31, no. 6, pp. 1261–1280, 2015.

[2] P. E. Dupont, B. J. Nelson, M. Goldfarb, B. Hannaford, A. Menciassi, M. K. O'Malley, N. Simaan, P. Valdastri, and G.-Z. Yang, "A decade retrospective of medical robotics research from 2010 to 2020," *Science Robotics*, vol. 6, no. 60, p. eabi8017, 2021. [Online]. Available: https://www.science.org/doi/abs/10.1126/scirobotics.abi8017

[3] Y. Kim and X. Zhao, "Magnetic soft materials and robots," *Chemical Reviews*, vol. 0, no. 0, p. null, 0, pMID: 35104403. [Online]. Available: https://doi.org/10.1021/acs.chemrev.1c00481

[4] T. da Veiga, J. H. Chandler, P. Lloyd, G. Pittiglio, N. J. Wilkinson, A. K. Hoshiar, R. A. Harris, and P. Valdastri, "Challenges of continuum robots in clinical context: a review," *Progress in Biomedical Engineering*, vol. 2, no. 3, p. 032003, aug 2020.

[5] L. Pancaldi, L. Noseda, A. Dolev, A. Fanelli, D. Ghezzi, A. J. Petruska, and M. S. Sakar, "Locomotion of sensor-integrated soft robotic devices inside sub-millimeter arteries with impaired flow conditions," *Advanced Intelligent Systems*, vol. n/a, no. n/a, p. 2100247. [Online]. Available: https://onlinelibrary.wiley.com/doi/abs/10.1002/aisy.202100247

[6] J. Edelmann, A. J. Petruska, and B. J. Nelson, "Magnetic control of continuum devices," *The International Journal of Robotics Research*, vol. 36, no. 1, pp. 68–85, 2017.

[7] Y. Kim, G. A. Parada, S. Liu, and X. Zhao, "Ferromagnetic soft continuum robots," *Science Robotics*, vol. 4, no. 33, p. eaax7329, 2019.

[8] M. Hidalgo, S. Cascinu, J. Kleeff, R. Labianca, J.-M. Löhr, J. Neoptolemos, F. X. Real, J.-L. Van Laethem, and V. Heinemann, "Addressing the challenges of pancreatic cancer: future directions for improving outcomes," *Pancreatology*, vol. 15, no. 1, pp. 8–18, 2015.

[9] M. Sugimoto, S. Takahashi, M. Kojima, N. Gotohda, Y. Kato, S. Kawano, A. Ochiai, and M. Konishi, "What is the nature of pancreatic consistency? assessment of the elastic modulus of the pancreas and comparison with tactile sensation, histology, and occurrence of postoperative pancreatic fistula after pancreaticoduodenectomy." *Surgery*, vol. 156(5), p. 1204–1211, 2014.

[10] I. Levental, P. C. Georges, and P. A. Janmey, "Soft biological materials and their impact on cell function," *Soft Matter*, vol. 3, pp. 299–306, 2007. [Online]. Available: http://dx.doi.org/10.1039/B610522J

[11] Y. Chitalia, S. Jeong, J. Bok, V. Nguyen, S. Melkote, J. J. Chern, and J. P. Desai, "Towards the design and development of a pediatric neuroendoscope tool," in *2019 IEEE/RSJ International Conference on Intelligent Robots and Systems (IROS)*, 2019, pp. 2998–3004.

[12] E. Diller, J. Zhuang, G. Zhan Lum, M. R. Edwards, and M. Sitti, "Continuously distributed magnetization profile for millimeter-scale elastomeric undulatory swimming," *Applied Physics Letters*, vol. 104, no. 17, p. 174101, 2014.

[13] G. Z. Lum, Z. Ye, X. Dong, H. Marvi, O. Erin, W. Hu, and M. Sitti, "Shape-programmable magnetic soft matter," *Proceedings of the National Academy of Sciences*, vol. 113, no. 41, pp. E6007–E6015, 2016.

[14] P. Lloyd, A. K. Hoshiar, T. da Veiga, A. Attanasio, N. Marahrens, J. H. Chandler, and P. Valdastri, "A learnt approach for the design of magnetically actuated shape forming soft tentacle robots," *IEEE Robotics and Automation Letters*, vol. 5, no. 3, pp. 3937–3944, 2020.

[15] M. Richter, V. K. Venkiteswaran, and S. Misra, "Multi-point orientation control of discretely-magnetized continuum manipulators," *IEEE Robotics and Automation Letters*, vol. 6, no. 2, pp. 3607–3614, 2021.

[16] G. Pittiglio, P. Lloyd, T. da Veiga, O. Onaizah, C. Pompili, J. Chandler, and P. Valdastri, "Patient-specific magnetic catheters for atraumatic autonomous endoscopy," *Soft Robotics*, 2022.

[17] P. Lloyd, G. Pittiglio, J. H. Chandler, and P. Valdastri, "Optimal design of soft continuum magnetic robots under follow-the-leader shape forming actuation," in *2020 International Symposium on Medical Robotics (ISMR)*, 2020, pp. 111–117.

[18] P. Lloyd, Z. Koszowska, M. Di Lecce, O. Onaizah, J. H. Chandler, and P. Valdastri, "Feasibility of fiber reinforcement within magnetically actuated soft continuum robots," *Frontiers in Robotics and AI*, vol. 8, 2021. [Online]. Available: https://www.frontiersin.org/article/10.3389/frobt.2021.715662

[19] L. Barducci, G. Pittiglio, J. C. Norton, K. L. Obstein, and P. Valdastri, "Adaptive dynamic control for magnetically actuated medical robots," *IEEE robotics and automation letters*, vol. 4, no. 4, pp. 3633–3640, 2019.

[20] R. J. Webster and B. A. Jones, "Design and kinematic modeling of constant curvature continuum robots: A review," *International Journal of Robotics Research*, vol. 29, no. 13, pp. 1661–1683, 2010.

[21] B. Siciliano, L. Sciavicco, L. Villani, and G. Oriolo, *Robotics: Modelling, Planning and Control*. Springer Publishing Company, Incorporated, 2010.

[22] F. Connolly, P. Polygerinos, C. J. Walsh, and K. Bertoldi, "Mechanical programming of soft actuators by varying fiber angle," *Soft Robotics*, vol. 2, no. 1, pp. 26–32, 2015.

[23] O. Strobel, J. Neoptolemos, D. Jäger, and M. Büchler, "Optimizing the outcomes of pancreatic cancer surgery." *Nat Rev Clin Oncol.*, vol. 16(1), pp. 11–26, 2019, pMID: 30341417.

[24] L. Blanc, A. Delchambre, and P. Lambert, "Flexible medical devices: Review of controllable stiffness solutions," *Actuators*, vol. 6, no. 3, 2017. [Online]. Available: https://www.mdpi.com/2076-0825/6/3/23

[25] D. Teilum, "In vitro measurement of the length of the sphincter of oddi." *Endoscopy*, no. 23(3), p. 114–116, 1991.

[26] S. Horiguchi and T. Kamisawa, "Major duodenal papilla and its normal anatomy." *Dig Surg*, no. 27, pp. 90–93, 2010.

[27] H. Ismail, C. G. Pretty, M. Signal, M. Haggers, C. Zhou, and J. G. Chase, "Mechanical behaviour of tissue mimicking breast phantom materials." *Biomedical Physics & Engineering Express*, vol. 3, p. 045010, 2017.

[28] Z. Liu, M. Li, X. Dong, Z. Ren, W. Hu, and M. Sitti, "Creating three-dimensional magnetic functional microdevices via molding-integrated direct laser writing," *Nature Communications*, vol. 13, p. 2016, 2022.